Flyback-based Input Series Converter as a Wide Input Auxiliary Power Supply

Thomas, A.J.; Mirzadarani, R.; Ghaffarian Niasar, M.

DOI
10.30420/566541398

Publication date
2025

Document Version
Accepted author manuscript

Published in
International Exhibition and Conference for Power Electronics, Intelligent Motion, Renewable Energy and Energy Management, PCIM Europe 2025

pcim
EUROPE

Flyback-based Input Series Converter as a Wide Input Auxiliary Power Supply

Ashish John Thomas [1], Reza Mirzadarani [1], Mohamad Ghaffarian Niasar [1]

[1] High Voltage Technologies, TU Delft, The Netherlands

Corresponding author: Ashish John Thomas, ashish.thomas@tennet.eu
Second author: Mohamad Ghaffarian Niasar, M.GhaffarianNiasar@tudelft.nl
Speaker: Ashish John Thomas, ashish.thomas@tennet.eu

Abstract

This paper presents the prototype development and performance evaluation of a three-stage flyback-based Input Series Converter designed as an Auxiliary Power Supply (APS) for a Modular Multilevel Converter (MMC)-based Arbitrary Waveform Generator (AWG). The APS is connected across the submodule capacitors of the MMC and converts the capacitor voltage to 24V, providing power to the gate drivers and control units within each submodule. The proposed converter features integrated active Input Voltage Sharing (IVS), a scalable architecture, and wide-input voltage operation. A multi-winding flyback transformer ensures high-voltage insulation between the submodule capacitor and the APS output while facilitating active IVS for balancing input capacitor voltages. A transformer prototype has been developed and tested in an open-loop converter configuration. The system's performance has been evaluated at an output power of 30W across an input voltage range of 300V–3600V.

1 Introduction

The massive penetration of renewable energy has increased the number of Power Electronic Interfaces (PEIs) in the grid. The waveforms generated by these PEIs are not perfectly sinusoidal and contain harmonics. Hence, the insulation of High Voltage (HV) equipment in the grid is experiencing new electrical stresses. Therefore, testing the insulation of HV equipment with a variety of electrical stresses will be beneficial to ensure reliable operation.
An MMC-based AWG has been developed in the High Voltage Lab at TU Delft to test a variety of HV equipment for dielectric strength, partial discharge behavior, and dielectric losses with complex waveforms [1]. The submodules (SM) in the MMC have Gate-Drive Units (GDUs) and Distributed Control Units (DCUs) that require power. This power is typically obtained from the SM capacitor. Depending on the test voltage level, the SM capacitor voltage can vary over a large range. Furthermore, the GDUs and DCUs operate at a low voltage, in the order of volts while the test voltage level, and thereby the SM capacitor voltage level is in the order of kilovolts. Hence, a wide-input, large step down converter is needed to serve as an APS.
Single-switch converter topologies such as flyback are typically used for designing an APS because of their simple structure and low cost. However, there exist a few Silicon-based MOSFETs rated at high voltages above 2000V with high on-state resistance and long voltage rise and fall times. When operated at a low duty cycle ($<$10%) at a high switching frequency, these switches do not turn-off completely. Hence, invariably some sort of series-connected switch topology needs to be used for designing an APS for HV applications. Such a design needs to have an effective voltage balancing methodology, circuitry for synchronized gate signals and scalable.

2 Topology Overview

Voltage imbalance between switches can occur in series-connected switches. This will result in reduced reliability and lifetime of the converter. The voltage imbalance could mainly be attributed to variations in MOSFET intrinsic parameters, mismatch in gate driving circuitry and external parasitics such as capacitance to ground through the heatsink [2]. A topology that provides an auto-balancing mechanism, using a flyback-based converter, with multiple primary stages, is presented in [3]. All the primary

windings, and the secondary winding are wound around the same transformer core, and is shown in Figure 1. Henceforth in this report, S1 refers to the upper switch, S2 to the middle one, and S3 to the bottom switch. The associated circuitry around the MOSFETs will also be named accordingly. Without an additional control strategy, the voltage across the MOSFETs are balanced by coupling of the primary windings in the transformer. The efficiency of the converter is higher as no passive circuit is used for balancing purposes.

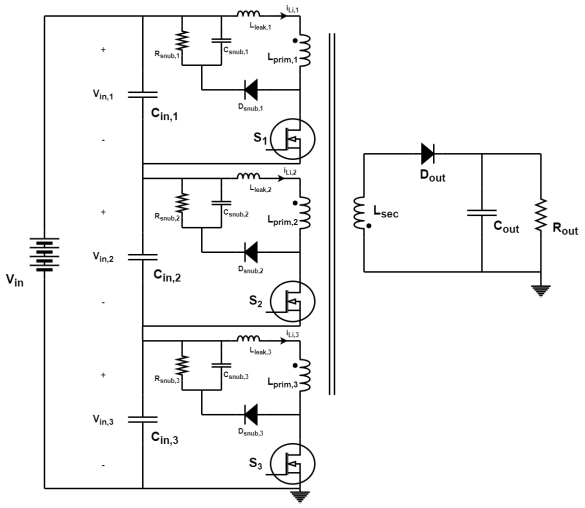

Fig. 1: 3 Stage Flyback-based Input Series Converter

The IVS procedure is analytically explained for the 3 Stage converter. The voltage across the input capacitors is given by Equation 1. x, y, z can be used interchangeably for any of the three input stages. L_{ixx} are the self-inductances of the primary windings, and M_{xy} and M_{xz} are the mutual inductances. i_{Lix}, i_{Liy}, and i_{Liz} are the currents through the 3 inductors.

$$V_{in,x}(t) = L_{ixx}\frac{di_{Lix}(t)}{dt} + M_{xy}\frac{di_{Liy}(t)}{dt}M_{xz} + \frac{di_{Liz}(t)}{dt} \quad (1)$$

If we assume that the voltage across one of the input capacitors is ΔV_{in} greater than that across the other capacitors, it can be proven that during the on state of the MOSFET, the input capacitor with higher voltage discharges faster, and the other capacitors in turn discharge slower, and this reduces the difference in voltage as given by Equation 2 over time. Here, t_0 is the time the MOSFET is turned on, and k is the coupling factor. If there is a difference between the voltage across input capacitors, the voltage will resonate with a constant frequency, with decreasing amplitude in each period due to resistance in the circuit. A large coupling factor k will increase the resonant frequency and hence speed of balancing [3].

$$\Delta V_{in}(t - t_0) = \Delta V_{in}(t_0)cos\frac{t - t_0}{\sqrt{(1-k)L_{ixx}C_{in,x}}} \quad (2)$$

The active IVS process takes place only when the primary windings are coupled in the integrated transformer and during the off-time of the switch there is no integrated voltage balancing taking place. If a particular MOSFET in the series chain is turned off earlier than the other MOSFETs, this MOSFET will block a higher voltage than the other MOSFETs. Therefore, care must be taken in designing a synchronous gate driver.

3 Design & Methodology

3.1 Resin Impregnated Paper Insulation Test

For the proposed auxiliary power supply, high-voltage (HV) insulation is required between the submodule capacitor and the converter output. This insulation is provided by the Flyback transformer, making its design crucial. The primary winding uses AWG26 magnet wire with a breakdown strength of 4.16 kV, which is insufficient for the designed converter, particularly under switching transients. To enhance insulation performance, Resin Impregnated Paper (RIP) is investigated. A test is conducted to evaluate the insulation improvement achieved using RIP. The evaluation follows the Applied Voltage Test specified in IEC 60076-3, with slight modifications.

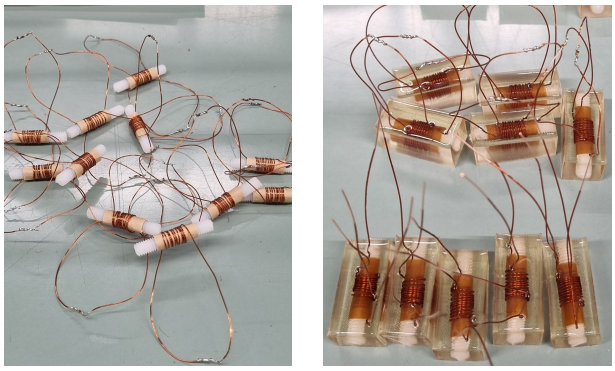

(a) (b)

Fig. 2: Breakdown test samples: (a) air-insulated, (b) epoxy resin CY225-insulated

Five different types of samples were prepared, each consisting of two windings wound over each other:

three air-insulated samples with no paper insulation, one layer of Kraft paper (0.15 mm thickness), and two layers of Kraft paper; and two epoxy resin-impregnated samples with one and two layers of Kraft paper, respectively. Each sample contained two windings of 10 turns each, and 11 samples were fabricated per configuration. During testing, the windings were shorted, with voltage applied to one winding while the other was grounded to assess the insulation system's strength. The air-insulated and epoxy resin-impregnated samples are depicted in Figure 2. The test was conducted at 50 Hz with a voltage ramp rate of approximately 150 V/s.

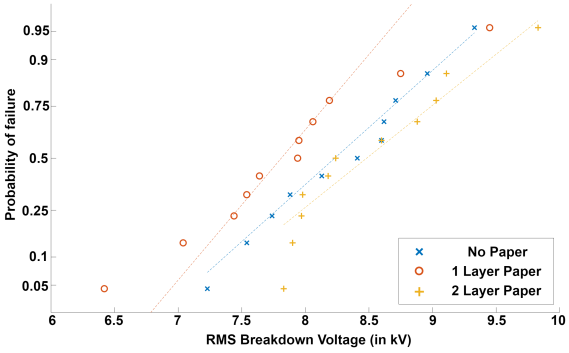

(a) Air-insulated samples results

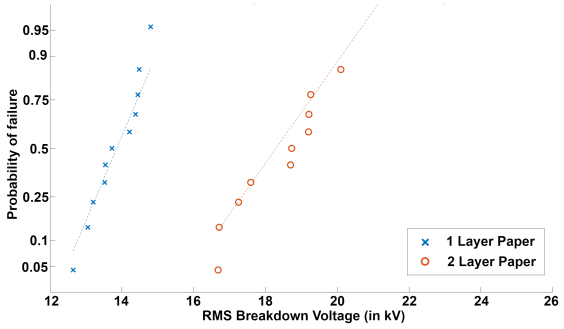

(b) Epoxy resin CY225-insulated samples results

Fig. 3: Normal probability plots for breakdown tests

A normal probability plot was used to assess the statistical distribution of breakdown voltages. Figure 3 shows the normal probability plots for air-insulated and epoxy resin-impregnated samples. The results indicate that air-insulated samples without paper closely follow the normal distribution, whereas those with one or two paper layers exhibit greater variance, particularly at lower voltages. This variability is attributed to the presence of air bubbles, which introduce non-deterministic behavior in breakdown performance.
Conversely, the samples impregnated with epoxy resin exhibit more uniform adherence to the normal distribution, implying a more deterministic breakdown behavior. Additionally, increasing the number of paper layers significantly enhances breakdown strength. The average breakdown voltage for samples with two layers of paper in epoxy resin more than doubles that of air-insulated counterparts.
Based on these findings, the Flyback transformer in this study will be encapsulated in epoxy resin CY225 to enhance dielectric strength. Although epoxy resin insulation affects the transformer's thermal performance, this is not a major concern given the auxiliary power supply's low power rating (30 W). The resulting losses are minimal, and the expected temperature rise remains within acceptable limits.

3.2 Flyback Transformer Design

The transformer core selection was based on the area product method, leading to the choice of the Ferroxcube ETD49/25/16 core with an area product of $A_p = 5.76$ cm^4 [4]. The ferrite core material used is Ferroxcube 3C97. The primary and secondary windings utilize AWG26 and AWG21 wire, respectively, selected to minimize skin effect losses while maintaining a current density of approximately 4 A/mm^2. The primary and secondary turns were determined as 120 and 30, respectively, based on magnetizing inductance, turns ratio, and the required air gap for energy storage.

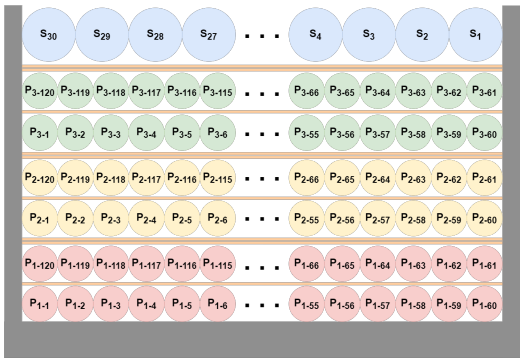

Fig. 4: Multi-winding Flyback Transformer Winding Configuration

The AC resistance, and consequently the copper losses, were estimated using Dowell's equation, yielding a total winding loss of $P_w = 0.94$ W. Core losses were computed via the Steinmetz equation, resulting in an estimated loss of $P_c = 0.29$ W under operating conditions. Simulations conducted in Ansys Maxwell confirmed that the simulated losses closely align with analytical calculations.

Due to space constraints, the 120-turn primary winding could not be accommodated in a single bobbin layer and was distributed across two layers. A C-type winding configuration was selected for its cost-effectiveness and ease of implementation. A layer-by-layer winding structure was adopted, with the primary windings arranged sequentially from the inner to the outer layers, and the secondary winding placed in the outermost layer. This configuration is illustrated in Figure 4.

To ensure adequate insulation, two layers of insulating paper were applied between the primary and secondary windings, as well as between adjacent primary windings. A single layer of insulation was used between layers within the same primary winding to prevent excessive separation, which could degrade the coupling coefficient. The chosen insulation strategy meets the design specifications while preserving the required magnetic coupling.

The transformer was fabricated and encapsulated in epoxy resin, as shown in Figure 5. Electrical characterization was performed using the Omicron Lab Vector Network Analyzer Bode 100 to accurately measure magnetizing inductance, leakage inductance, and DC resistance. The key electrical parameters are summarized in Table 1. The measured air gap was approximately $l_g = 0.6$ mm. The coupling factor analysis reveals that as the primary windings are positioned closer to the secondary, their coupling improves slightly. Minor variations in coupling factors among the primary windings were observed, but remain within acceptable limits.

	Primary 1	Primary 2	Primary 3	Secondary
Magnetizing Inductance	3.82 mH	3.78 mH	3.84 mH	239.73 μH
Leakage Inductance	65.07 μH	48.76 μH	13.33 μH	1.58 μH
DC Resistance	1.614 Ω	1.476 Ω	1.756 Ω	175.2 mΩ
Coupling Factor k_1 to Secondary	0.9915	0.9935	0.9983	-
Coupling Factor k_2 (P1-P2)	0.9946			
Coupling Factor k_3 (P2-P3)	0.9943			
Coupling Factor k_4 (P3-P1)	0.9875			

Tab. 1: Prototype Transformer Electrical Specifications

Given the high voltage stress in the Flyback transformer, the innermost primary winding, which experiences the highest voltage relative to ground, was assigned to the MOSFET operating at the highest potential. The breakdown voltage test was conducted by applying high voltage to this winding while grounding the secondary. The transformer exhibited a breakdown voltage of 32.88 kV—substantially exceeding the converter's maximum operational voltage. The breakdown occurred within the epoxy insulation near the high-voltage terminals.

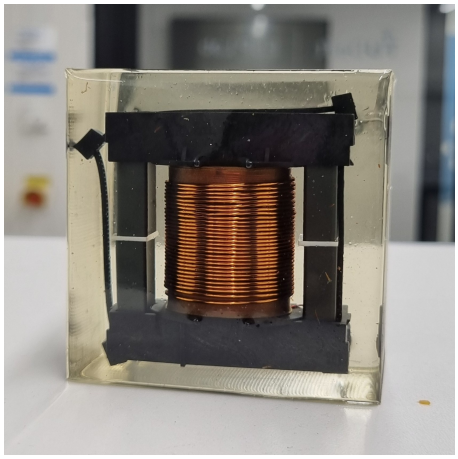

Fig. 5: Prototype Flyback Transformer

3.3 Converter Prototype Development

The gate driving circuit for the series-connected MOSFETs is based on the methodology introduced in [5], which ensures a constant negative turn-off voltage—critical for SiC MOSFETs—and minimizes oscillations to prevent false triggering. A gate transformer is essential for isolating the low-voltage gate pulse generation circuit from the APS power stage, as two MOSFET sources are floating above ground potential.

The transformer consists of a single primary winding driven by a PWM controller and three physically separated cores, each with a secondary winding connected between the gate and source of its respective switch. This approach, proposed in [6], suggests that increasing the number of cores reduces the coupling coefficient. To mitigate this, a compensation capacitor is added to the primary side, and the secondary windings have a higher turn count than the primary to maintain a 1:1 voltage transfer ratio.

For PWM gate pulse generation, an Arduino Uno R3 produces a 5V PWM signal and its complementary counterpart, with the duty cycle adjustable between 1% and 50% via a potentiometer connected to an analog input. These signals drive the ST STGAP2SICSN gate driver IC, which converts the 5V logic level into a 15V gate drive voltage. To prevent damage to the IC, the 15V output drives a MOSFET totem-pole circuit, which in turn powers the gate transformer primary through a damping resistor and compensation capacitor.

The fully assembled gate drive circuit and three-

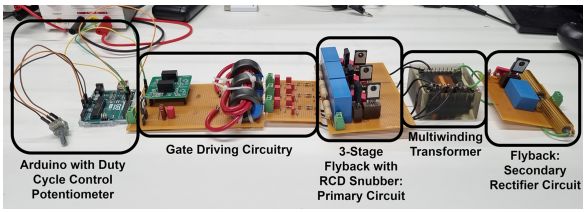

Fig. 6: Three-Stage Flyback-Based Input Series Converter

stage input-series flyback converter are shown in Figure 6. For testing, the load is assumed to be purely resistive. During the rectifier diode's reverse recovery, it momentarily behaves as a capacitor, resonating with the secondary leakage inductance. To suppress this effect, an RC snubber circuit is implemented across the diode. The components used in the APS prototype are listed in Table 2.

Component	Manufacturer	Function
C2M1000170D-ND	Wolfspeed, Inc.	1.7kV SiC Flyback Converter MOSFETs
1697-C6D05170H-ND	Wolfspeed, Inc.	1.7kV, 5A RCD Snubber, Output Diode
PHE845VW7100MR06L2	TDK Electronics	1μF, 1.5kV DC Input Filter Capacitor
B32526T1476K000	TDK Electronics	4.7μF, 100V DC Output Capacitor
B64290A0659X830	TDK Electronics	7μH Ferrite Core for Driving Transformer
150kΩ	-	RCD Snubber Resistor
3.3nF	-	RCD Snubber Capacitor
30W 20Ω	-	Output Resistor

Tab. 2: Components used for APS Prototype

4 Results

The designed converter operates at an output power of 30W, maintaining a stable 24V output across an input voltage range of 300V–3600V. Experimental validation was conducted at multiple input voltage levels to assess performance.

Gate voltages of the three MOSFETs were measured using a differential probe. An example, with the duty cycle of 19.1% and V_{in}=1200V is shown in Figure 7. A spike was observed in the gate pulse during turn-on due to the gate-drive transformer's leakage inductance, while turn-off oscillations resulted from interactions between the flyback transformer's leakage inductance and the MOSFET's output capacitance C_{oss}. Switch S3 turned on slightly faster, leading to a higher on-state voltage, whereas S2 switched off first, resulting in a lower turn-off voltage.

The flyback transformer's winding configuration affects leakage inductance distribution. The innermost winding, connected to S2, exhibits the highest leakage inductance, leading to greater energy dissipation in the snubber circuit and higher snubber capacitor voltage. At $V_{in} = 1200V$, input capacitor

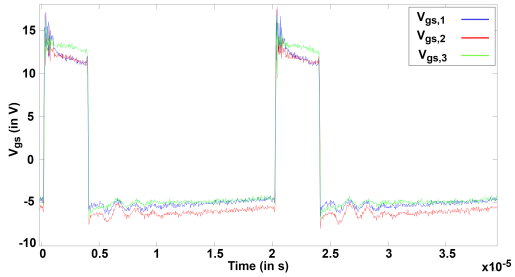

Fig. 7: V_{gs} for $V_{in} = 1200V$ & $D = 0.191$

voltage deviation from the ideal 400V per capacitor is limited to 6.58V, with the second capacitor showing the highest voltage (Figure 8). The snubber capacitor, MOSFET, and input capacitors form a loop, resulting in voltage imbalances due to leakage inductance variations.

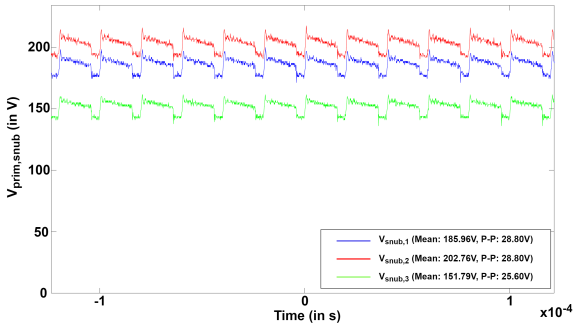

(a) Snubber Capacitor Voltage

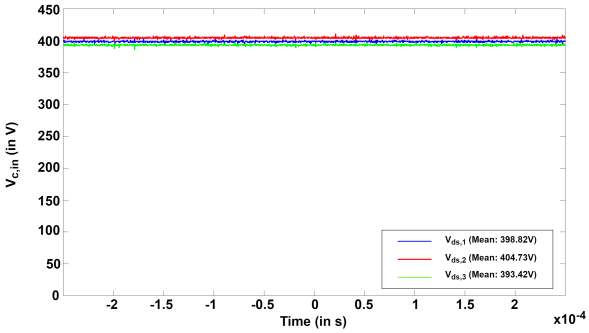

(b) Input Capcitor Voltage Sharing

Fig. 8: Snubber and Input Capacitor Voltages for V_{in}=1200V

MOSFET blocking voltages were analyzed across different input conditions (Figure 9). Oscillations of similar amplitude and frequency were present at all voltage levels due to interactions between the primary leakage inductance and MOSFET output capacitance. Steady-state results showed minor voltage imbalances, with $V_{ds,2} > V_{ds,1} > V_{ds,3}$, influenced by slight differences in transformer turns ratios and input capacitor voltage distribution. Despite

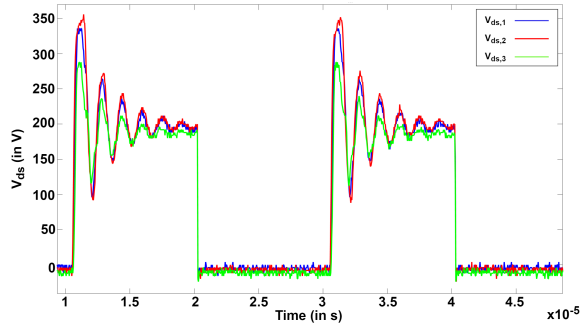

(a) V_{ds} for $V_{in} = 300V$ & $D = 0.517$

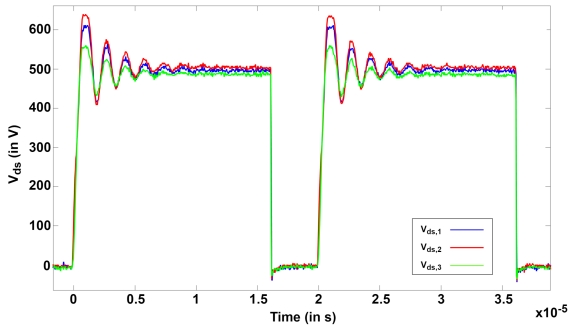

(b) V_{ds} for $V_{in} = 1200V$ & $D = 0.191$

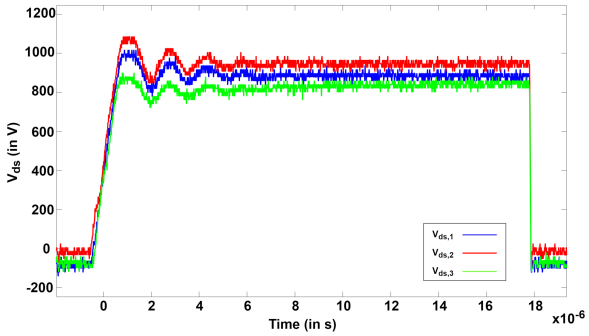

(c) V_{ds} for $V_{in} = 2400V$ & $D = 0.11$

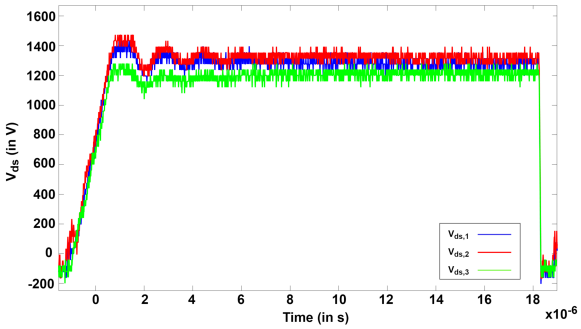

(d) V_{ds} for $V_{in} = 3600V$ & $D = 0.077$

Fig. 9: Flyback Converter Switch Blocking Voltage at different operating points

these imbalances, the converter achieved effective voltage sharing without additional active or passive balancing circuitry. Due to the unavailability of differential probes with sufficient voltage isolation,V_{ds} measurements at $V_{in} = 2400V$ and $V_{in} = 3600V$ were conducted using standard probes connected to the drain pins and referenced to ground, and subtracting the voltage across the input capacitors on MATLAB. Additionally, minor calibration errors in the probes introduced slight inaccuracies, evident from the small negative voltage values observed during the MOSFET on-state.

Converter efficiency decreased from 96.2% at $V_{in} = 300V$ to approximately 50% at $V_{in} = 3600V$. This drop is primarily due to increased MOSFET and output diode switching losses at higher voltages, as well as elevated temperatures leading to higher $R_{ds,on}$ and conduction losses. Future improvements could focus on enhanced thermal management, faster gate drivers, and replacing the secondary-side diode with a MOSFET synchronous rectifier for reduced switching losses.

Figure 10 presents the converter's output voltage. Leakage inductance-induced spikes were observed, which could be mitigated by increasing the output capacitance. The mean and peak-to-peak voltage values confirm stable operation.

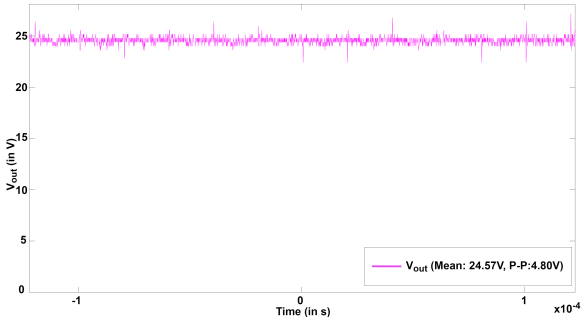

Fig. 10: APS Output Voltage

5 Conclusions

This paper presents the development of a low-power, wide-input flyback-based Input Series Converter designed as an auxiliary power supply for MMC submodules. The converter successfully operates across an input range of 300V–3600V while maintaining a constant 24V output. However, efficiency declines at higher input voltages due to extended switching times of the MOSFETs and output diode. The flyback-based input series topology inherently balances voltage across input capacitors and MOSFETs by coupling transformer primary windings on a shared core. High-voltage insulation is achieved using RIP within the transformer.

Future work should explore alternative winding con-

figurations, LC snubber circuit design, improved heat management, and enhanced gate driving circuits for better synchronization and efficiency.

References

[1] D. A. Ganeshpure, T. B. Soeiro, M. Gagic, M. G. Niasar, P. Bauer, and P. Vaessen, "Demonstration of scalable series-connected submodule of modular-multilevel-converter- based arbitrary wave shape generator used for high-voltage testing from off-the-shelf component," *IEEE Open Journal of the Industrial Electronics Society*, vol. 4, pp. 371–386, 2023. DOI: 10.1109/OJIES.2023.3310403.

[2] K. Vechalapu, S. Bhattacharya, and E. Aleoiza, "Performance evaluation of series connected 1700v sic mosfet devices," in *2015 IEEE 3rd Workshop on Wide Bandgap Power Devices and Applications (WiPDA)*, 2015, pp. 184–191. DOI: 10.1109/WiPDA.2015.7369327.

[3] T. Meng, C. Li, H. Ben, and J. Zhao, "An input-series flyback auxiliary power supply scheme based on transformer-integration for high-input voltage applications," *IEEE Transactions on Power Electronics*, vol. 31, no. 9, pp. 6383–6393, 2016. DOI: 10.1109/TPEL.2015.2505322.

[4] "Etd49/25/16." (2008), [Online]. Available: https://ferroxcube.home.pl/prod/assets/etd49.pdf.

[5] G. Yu, M. G. Niasar, D. Ganeshpure, T. B. Soeiro, and P. Bauer, "A transformer isolated driving method for sic mosfets with a constant negative off voltage," in *2021 IEEE 19th International Power Electronics and Motion Control Conference (PEMC)*, 2021, pp. 39–45. DOI: 10.1109/PEMC48073.2021.9432530.

[6] S. Ghafoor, M. Kulkarni, R. Mirzadarani, P. Vaessen, and M. G. Niasar, "A scalable isolated gate driver with programmable frequency and duty cycle for series-connected sic mosfets," *IEEE Open Journal of the Industrial Electronics Society*, vol. 6, pp. 95–114, 2025. DOI: 10.1109/OJIES.2024.3521325.